energies

MDPI

Article

Hydrogen Production System through Dimethyl Ether Autothermal Reforming, Based on Model Predictive Control

Tie-Qing Zhang, Seunghun Jung * and Young-Bae Kim *

Department of Mechanical Engineering, Chonnam National University, Gwangju 500010, Republic of Korea
* Correspondence: shjung@jnu.ac.kr (S.J.); ybkim@chonnam.ac.kr (Y.-B.K.); Tel.: +82-625-301-677 (Y.-B.K.); Fax: +82-062-530-1689 (Y.-B.K.)

Abstract: In this study, a thermodynamic analysis of the low temperature autothermal reforming (ATR) of dimethyl ether (DME) for hydrogen production was conducted. The $Pd/Zn/\gamma\text{-}Al_2O_3$ catalyst coated on the honeycomb cordierite ceramic was applied to catalyze the reaction, and the optimum activity temperature of this catalyst was demonstrated experimentally and through simulations to be 400 °C. Furthermore, an optimal model predictive control (MPC) strategy was designed to control the hydrogen production rate and the catalyst temperature. Experimental and simulation results indicated that the controller was automated and continuously reliable in the hydrogen production system. By establishing the state-space equations of the autothermal reformer, it can precisely control the feed rates of DME, high-purity air and deionized water. Ultimately, the hydrogen production rate can be precisely controlled when the demand curve changed from 0.09 to 0.23 mol/min, while the catalyst temperature was maintained at 400 °C, with a temporary fluctuation of 4 °C during variations of the hydrogen production rate. Therefore, the tracking performance of the hydrogen production and the anti-disturbance were satisfactory.

Keywords: autothermal reforming; model predictive control; dimethyl ether; hydrogen production; temperature control

Citation: Zhang, T.-Q.; Jung, S.; Kim, Y.-B. Hydrogen Production System through Dimethyl Ether Autothermal Reforming, Based on Model Predictive Control. *Energies* **2022**, *15*, 9038. https://doi.org/10.3390/en15239038

Academic Editors: Yanzhou Qin, Yulin Wang and Xiao Ma

Received: 4 November 2022
Accepted: 26 November 2022
Published: 29 November 2022

1. Introduction

In recent years, the worldwide energy demand has increased significantly as the world's population has grown, financial conditions have evolved, and urbanization has accelerated [1–4]. However, the traditional energy supply method relies on the exploitation of fossil energy, which is limited by the uneven geographical distribution and inconsistent exploitation difficulty. At the same time, long-term consumption makes fossil energy increasingly scarce, and reducing carbon emissions has become a global issue [5,6]. In terms of energy supply innovation, the proportion of new clean energy represented by hydrogen, solar energy and biomass (e.g., biogas and biodiesel) in the overall energy supply field is increasing annually, and fuel cell vehicles are cleaner and more efficient than traditional internal combustion engine vehicles [7,8]. Electric vehicles are an eco-friendly transportation method, but due to the relatively long charging time, the risk of explosion, and high cost of replacing batteries, hydrogen vehicles have attracted attention as a next generation transportation method. These situations indicate the urgent need to develop clean and renewable energy to replace the existing energy supply system, leading to greater attention to the research and development of hydrogen energy [9].

Hydrogen power generation is a prospective solution to the energy storage of green energy for a completely clean and efficient hydrogen industry [10], which can provide clean, efficient, reliable, and affordable energy with significant societal benefits [11]. Hydrogen energy thus plays an important role in achieving sustainable development goals (SDGs) on a global scale. However, the hydrogen energy industry has characteristics of multiple components, complex technical routes, diverse application scenarios, and high economic

costs. These are the major obstacles that affect the progress of the hydrogen industry. The economics of hydrogen requires the strong cross-chain cooperation to be manifested. With the continuous advancement of technology and the expansion of the scale of the hydrogen energy industry, the marginal cost has been gradually accepted by society.

Types of hydrogen-based systems can be classified, according to the end user [12]. Ahmed et al. [13] systematically studied the use of hydrogen fuel in the Malaysian transportation system for a sustainable and environmentally friendly future. Hou T F et al. [14] presented a facile fabrication process to enhance the photoelectrochemical(PEC) performance of ZnO-based photoelectrodes for the conduct of solar water splitting for hydrogen generation. Bellotti et al. [15] studied the feasibility of an innovative device that generates hydrogen on the grid through a water electrolysis unit and synthesized it with carbon dioxide stored in fossil fuel power plants to produce methanol. In terms of energy supply miniaturization, the proton exchange membrane fuel cells (PEMFCs) can be used for the efficient conversion of chemical and electrical energy. PEMFCs have the characteristics of a high energy density, absence of pollutants, and efficiency at relatively low temperatures and pressures. These conditions make PEMFCs an excellent solution for hydrogen utilization in recent years [7,16,17]. These studies demonstrate the practical solutions for hydrogen applications, but in portable applications, it has many drawbacks, in terms of safety and storage [18]. Therefore, to form a complete hydrogen industry chain, how to produce hydrogen efficiently and economically has become the core issue, which is increasing attention.

Hydrocarbon reforming is a widely used hydrogen production technology. Brown [19] compared the utility of seven common fuels as hydrogen sources for the proton exchange membrane fuel cells for automobile propulsion, which directly confirmed the wide range of feedstock required for the hydrogen production. Among many hydrocarbons, dimethyl ether, as a feedstock for the hydrogen production, has the following advantages:

(1) The sources of dimethyl ether are abundant and diverse. In recent years, hydrogen and carbon monoxide synthesis methods have been developed to replace the original costly methanol dehydration production method, resulting in a significant reduction in the cost of DME preparation and an increase in production efficiency, which is conducive to large-scale applications.

(2) Dimethyl ether is non-toxic and non-corrosive, and is easily degraded in the atmospheric troposphere, which ensures the environmental friendliness of dimethyl ether during use.

(3) Similar to liquefied petroleum gas (LPG), dimethyl ether can be compatible with the existing infrastructure of LPG and natural gas, which reduces the commercialization cost of dimethyl ether reforming to produce hydrogen, and greatly reduces the threshold for this new fuel to enter the energy market.

(4) Dimethyl ether is easily liquefied at about 5–6 atmospheres, making it easy to store and transport, which significantly reduces the transportation cost of the fuel.

(5) It has a higher hydrogen density than other commercial fuels (e.g., diesel) and can be reformed to release more of the hydrogen stored in it.

By integrating these advantages, DME is very attractive as a mobile hydrogen carrier for fuel cell systems [20,21].

Typical hydrocarbon-reforming technologies are steam reforming (SR), autothermal reforming (ATR), and partial oxidation (POX) [22–25]. Wu Z et al. [26] studied the methane steam reforming in a grille-sphere composite packed bed, and the effect of the diameter distribution of the particles in the packed bed reactor on the efficiency was investigated. Cherif A et al. [27] performed a thermodynamic analysis of the methane autothermal steam reforming for the hydrogen production, and a new configuration with 18 catalyst bed macrostructures alternately installed, was designed. ATR is thermally neutral in the reaction and a muffle furnace is only used to preheat the catalyst to the optimum temperature during the start-up phase, while no external heat source is required to keep the reaction to be carried out during the continuous operation. Furthermore, it has an

excellent hydrogen yield among the three methods. Therefore, ATR is an efficient and economical method of hydrogen production [28]. Hydrogen production by autothermal reforming of DME is significantly affected by the catalyst bed temperature; that is, under the same physical operating conditions, a higher reactor temperature theoretically leads to a higher hydrogen yield. However, a sustained high temperature can reduce the catalyst life and hydrogen production efficiency [29]. Many studies showed that excessively high temperatures are destructive to the physical structure of the reactor. Specifically, the prolonged exposure to 20 K over the design temperature halved the lifetime of the reformer tubes [30,31]. Meanwhile, the excessively high temperature in the POX may also lead to catalyst sintering [32]. Therefore, in addition to controlling the hydrogen production rate to meet the specific demands of the load, keeping the reformer operating at the optimum temperature during the autothermal reforming is necessary to supply hydrogen to on-board fuel cells.

In view of the hysteresis of the control action due to the chemical reaction of this system and the situation of the multiple inputs and outputs, many researchers have explored the control strategies. Dolanc et al. [33] developed a PID controller that keeps the reaction at a stable reactor temperature while accurately responding to the hydrogen demand for a specific load in the diesel autothermal reforming process. However, compared to the PID control, the model predictive control (MPC) performs better in the chemical industry, which makes MPC more capable of operating the hydrogen production under strict performance specifications and constraints [34]. From the perspective of the working mechanism of the model predictive control, its advantages are reflected in the following points:

(1) The model is easy to build. The process characterization can be detected by performing simple experiments and does not require a deep exploration of the chemical reaction mechanism.

(2) The discrete convolution and model described by non-minimization are used, and the information redundancy is large, which is beneficial to improve the robustness of the system.

(3) Using the rolling optimization strategy, the online optimization calculation is repeatedly performed, and the rolling execution is conducted to obtain a better dynamic control performance, to compensate for the uncertainty caused by the model mismatch, distortion and disturbance in time.

For instance, the hydrogen production rate and reactor temperature are simultaneously set as system constraints and controlled synchronously in the model predictive control, which has a positive significance for the system performance optimization and long-term stable operation. Similar control strategies have been applied in other devices for the hydrogen production. Kyriakides et al. [35] developed a MPC strategy for low temperature methane SR in membrane reactors, enabling the high methane conversion at relatively low temperature levels. Paliwal N K et al. [36] developed a MPC-based control scheme for a microgrid system, based on photovoltaic power generation, lead-acid battery energy storage and hydrogen production, resulting in a stable and efficient energy supply system. Hu et al. [37] demonstrated a nonlinear multivariable predictive controller with an excellent computational performance for the ATR reactors.

The above studies demonstrate the feasibility and superiority of the MPC in chemical reaction control processes. However, few studies have focused on the application of model predictive control in the autothermal reforming of dimethyl ether for hydrogen production so far, which is a highly integrated and efficient hydrogen production process. Inspired by this research, this study innovatively contracts an efficient DME autothermal reforming system, based on the MPC control and demonstrates its reliability and efficiency through simulation and experiments. Ultimately, this study prospectively applies model predictive control to the hydrogen production using DME, overcoming the hysteresis problem that is characteristic of the chemical reaction control processes. In addition, this system, when integrated with the hydrogen purification module, has the potential to be used in combination with an on-board fuel cell to power new energy vehicles, which is an important step in the promotion of hydrogen energy.

2. Mathematical Modelling and Control Method

2.1. ATR Reformer Model

MATLAB Simulink is applied to the simulation. Simulink plays an important role in the control strategy to linearize the complex chemical reaction system for the MPC control. In chemical kinetic models, Gibbs free energy is a generic function for identifying equilibrium states because of its concise properties. For the multi-matter and multi-phase systems, the equilibrium calculation can be performed by the Gibbs energy minimization method [38]. In this case, the Arrhenius equation to describe the rate of a chemical reaction is appropriate. The system is treated as a closed-loop one so that the equilibrium composition is related to the temperature and concentrations of the individual components in the reactions for a given catalyst performance. To facilitate the model operation, this study adopts the following assumptions:

(1) The overall DME autothermal reforming reaction can be divided into five steps: DME hydrolysis, methanol (MeOH) steam reforming, MeOH decomposition, MeOH partial oxidation, and carbon monoxide(CO) oxidation in which the heat generated by the exothermic reaction can provide energy for the endothermic reaction, making the entire reaction thermoneutral. The water gas shift (WGS) is integrated after the autothermal reformer so that the CO can be converted to carbon dioxide (CO_2) and generate more hydrogen. Various catalysts have been extensively studied and commercialized, and the conversion rate of Cu/Zn/γ-Al_2O_3 is higher than that of other commercial catalysts [39,40]. Therefore, a ternary Cu/Zn/γ-Al_2O_3 (Cu: 20 wt.%, Zn: 20 wt.%) catalyst was used in the reformer for the WGS.

(2) As the liquid water enters the reactor after passing through a 50 cm-long steel pipe that is heated to 150 °C by a heating belt, the liquid water is completely converted into vapor to participate in the reaction.

The mass balance of the mass transport can be described by the following equation [41]:

$$\epsilon_p \rho \frac{\partial \omega_j}{\partial t} + \nabla \cdot j_j + \rho (u \cdot \nabla) \omega_j = R_j \tag{1}$$

$$j_j = -\left(\rho \omega_j \sum_k D_{e,jk} d_k + D_{e,j}^T \frac{\nabla T}{T} \right) \tag{2}$$

$$D_{e,jk} = \frac{\epsilon_p}{\tau_F} D_{ik},\ D_{e,j}^T = \frac{\epsilon_p}{\tau_F} D_j^T,\ \tau_F = {\epsilon_p}^{-1/3} \tag{3}$$

$$d_k = \nabla x_k + \frac{1}{p_A}[(x_k - w_k) \nabla p_A] \tag{4}$$

$$x_k = \frac{\omega_k}{M_k} M_n\ ,\ M_n = \left(\sum_j \frac{\omega_j}{M_j} \right)^{-1} \tag{5}$$

Meanwhile, the energy balance of the mass flow can be described by the following equations:

$$A_c \left(\rho C_p \right)_{eff} \frac{\partial T}{\partial t} + A_c \rho_F C_{p,f} u \cdot \nabla T + \nabla \cdot q = Q \tag{6}$$

$$q = -A_c k_{eff} \nabla T \tag{7}$$

$$\left(\rho C_p \right)_{eff} = \theta_s \rho_s C_{p,s} + \epsilon_p \rho_f C_{p,f} \tag{8}$$

$$k_{eff} = \theta_s k_s + \theta_s k_f + k_{disp} \tag{9}$$

The boundary conditions at the reactor feed port $z = 0$ are as follows:

$$\omega_j = \omega_{j,o} \quad T = T_o \quad T_S = T_{s,o} \quad P = P_o \tag{10}$$

At the end of the reactor $z = L$, the boundary conditions can be defined as:

$$\frac{\partial \omega_j}{\partial z} = 0 \quad \frac{\partial T}{\partial z} = 0 \quad \frac{\partial T_s}{\partial z} = 0 \tag{11}$$

Initial conditions of the reaction are defined as:

$$\omega_j = \omega_{j,o} \quad T = T_o \quad T_S = T_{s,o} \tag{12}$$

Annotations of the parameters applied in the mass and energy balance model are shown in Table 1.

Table 1. Parameters applied in the Equations (1)–(12).

Parameters	Annotation	Unit
ω_i	Mass fraction of component j	-
A_c	Cross-sectional area of the channel	m^2
R_j	Overall reaction rate for component j	$mol/s/m^3$
ϵ_p	Catalyst porosity	-
τ_F	Effective transport factor	-
u	Fluid velocity	m/s
ρ	Fluid density	kg/m^3
Cp,s	Heat capacity of solid	$J/K/kg$
Cp,f	Heat capacity of gas	$J/K/kg$
q	Flux of heat	W/m^2
k_{eff}	Effective thermal conductivity	$W/m/K$
$(\rho Cp)_{eff}$	Heat capacity per unit volume	$J/m^3/K$
Q	Heat production rate per unit volume	W/m^3

Several institutes have developed the chemical kinetics of the autothermal reforming of DME [42–44]. Based on these studies, the individual steps of the reaction and kinetic equations used to describe the reaction rates are shown in Table 2, and the parameters can be found in Table 3.

Table 2. Reactions that take place in the DME autothermal reformer.

Reactions		Enthalpy	Kinetics of the Reactions
DME Hydrolysis	$CH_3OCH_3 + H_2O \rightarrow 2CH_3OH$	ΔH = 24 kJ/mol	$r_H = k_H \exp\left(\frac{-E_H}{RT}\right) C_{DME}$
MeOH SR	$CH_3OCH_3 + H_2O \rightarrow CO_2 + 3H_2$	ΔH = 49 kJ/mol	$r_{SR} = k_{SR} \exp\left(\frac{-E_{SR}}{RT}\right) C_{CH_3OH} C_{H_2O}$
MeOH Decomposition	$CH_3OH \rightarrow CO + H_2$	ΔH = 90.1 kJ/mol	$r_D = k_D \exp\left(\frac{-E_D}{RT}\right)$
Partial Oxidation	$CH_3OH + 1/2O_2 \rightarrow 2CO_2 + 2H_2$	ΔH = −193 kJ/mol	$r_{PO} = k_{PO} \exp\left(\frac{-E_{PO}}{RT}\right) C_{CH_3OH} C_{O_2}$
CO Oxidation	$CO + 1/2O_2 \rightarrow CO_2$	ΔH = −283 kJ/mol	$r_{COX} = k_{COX} \exp\left(\frac{-E_{COX}}{RT}\right) C_{CO}$
Water Gas Shift	$CO + H_2O \leftrightarrow CO_2 + H_2$	ΔH = −41.1 kJ/mol	$r_{WGS} = k_{WGS} \exp\left(\frac{E_{WGS}}{RT}\right)\left(P_{CO}\, P_{H_2O} - \frac{P_{CO_2}\, P_{H_2}}{k_{eq,WGS}}\right)$ $k_{eq,WGS} = \exp\left(\frac{-E_{eq,WGS}}{RT} - C_{eq,WGS}\right)$

In this multi-input multi-output (MIMO) control system, the catalyst temperature and hydrogen production rate are the objective variables. Therefore, they are fed back to the MPC controller for the feedback correction. The MPC then controls the DME, air, and vapor supply rates, according to the linearized space state equation of the reaction system, to meet specific hydrogen demands and stabilize the reactor temperature. Based on the mathematical description of the hydrogen generation system, the linearized Simulink model is shown in Figure 1.

Table 3. Reaction kinetic parameters.

Parameters	Annotation	Value	Unit
k_H	Pre-coefficient of Reaction i	1163.232	$m^3 \cdot s/kg_{cat}$
k_{SR}		154.7	$m^6/(mol \cdot s \cdot kg_{cat})$
k_D		99.7×10^3	$mol/(s \cdot kg_{cat})$
k_{PO}		400.5	$m^6/(mol \cdot s \cdot kg_{cat})$
k_{COX}		2.1×10^5	$m^3/(s \cdot kg_{cat})$
k_{WGS}		5000	$mol/(kg_{cat} \cdot s \cdot Pa^2)$
$C_{eq,WGS}$		3.33	-
E_H	Activation Energy of Reaction i	22.237	kJ/mol
E_{SR}		57.9	
E_D		110.8	
E_{PO}		54.9	
E_{COX}		63.3	
E_{WGS}		100	
$E_{eq,WGS}$		40	
R	Universal Gas Constant	8.314	J/K/mol
C_i	Concentration of Species i	-	mol/m^3
T	Temperature of Reactor	-	K

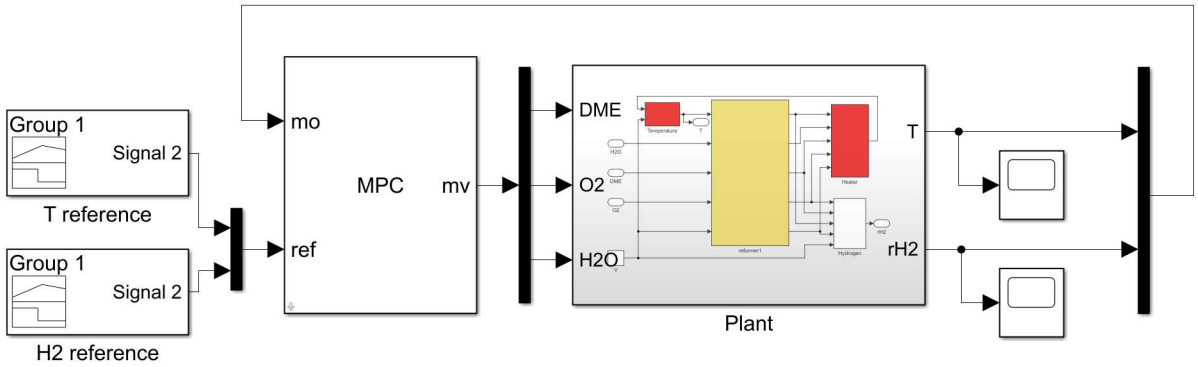

Figure 1. Schematic diagram of the MPC in Simulink.

2.2. State Space Equations Applied in the MPC

Considering that the hydrogen conversion is mainly affected by the catalyst temperature and the flexibility of the hydrogen supply is also crucial in the hydrogen supply of the on-board fuel cells, these two items are set as the control objectives of the control system. Furthermore, MPC is a robust control strategy. Since its inception in the 1970s, MPC has evolved into a new control algorithm characterized by diversity and usefulness. It has a wide range of applications in the chemical and mechanical fields because of its simplicity, richness, and practicality. MPC typically establishes a predictive model first, and then performs a rolling optimization and feedback correction. Once the model of the controlled plant is established, it can control multiple objective variables during its operation.

The implementation of MPC aims to model the optimization problem and then perform a rolling optimization to determine the final output of the controller. Typically, MPC relies on a linear time-invariant, discrete-time, state-space model of the system to predict the future response of the system. MPC requires solving the optimization problem through the repeated prediction and optimization at each time step. When the optimal solution of the optimization problem is obtained, it is used as the control action of the real actuator. Figure 2 illustrates the mechanism of a typical MPC controller.

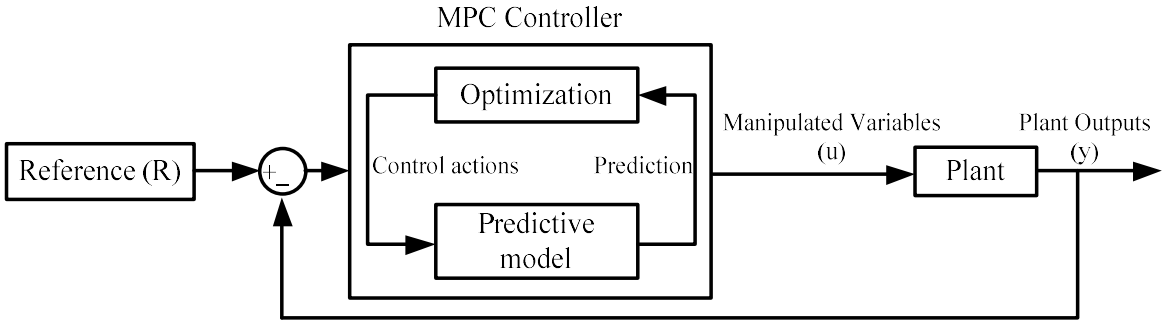

Figure 2. MPC controller mechanism.

Following the construction of a predictive model, the MPC can predict the future output characteristics of a control objective over a prediction horizon, and an optimum control sequence is obtained based on certain criteria. To ensure the optimality and reliability, only the first action in the control sequence is implemented [35,45,46]. The current control action is determined by solving a finite-time-domain open-loop optimal control problem at each sampling instant. The current state of the process is taken as the initial state of the optimal control problem and the obtained optimal control sequence only executes the first control action. Therefore, the flow rates of water, DME, and air are continuously optimized over time, based on the space state equation obtained by linearizing the ATR reformer model, which considers the effects of the ideal optimization and practical uncertainty in the future finite time domain. In the simulation, when determining the predictive horizon, it is gradually increased until further increases have a minor impact on the performance. The sampling time is typically determined as 10% of the prediction horizon. Finally, the prediction horizon and sampling time are determined to be 20 s and 2 s, respectively after trying many simulations. We obtained the linearized mathematical model of the plant model using the linear analysis tool in MATLAB. The continuous-time state-space model and the constant matrixes A, B, C, and D are listed as follows.

$$\begin{aligned} \dot{x} &= Ax + Bu \\ y &= Cx + Du \end{aligned} \tag{13}$$

where:

$$A = \begin{bmatrix} 4.663 \times 10^{-9} & -9.291 \times 10^{-9} & 1.398 \times 10^{-8} & -4.661 \times 10^{-9} & 4.658 \times 10^{-9} & 4.915 \times 10^{-13} \\ -0.2357 & 0.4692 & -0.7064 & 0.2356 & -0.2354 & -3.222 \times 10^{-5} \\ 0.0602 & -0.1205 & 0.1807 & -0.0602 & 0.0603 & -1.752 \times 10^{-6} \\ -0.118 & 0.2346 & -0.3535 & 0.1179 & -0.1178 & -1.922 \times 10^{-5} \\ 0.2299 & -0.4653 & 0.6918 & -0.2303 & 0.2308 & -7.84 \times 10^{-5} \\ 16.88 & 21.91 & 29.14 & -13.02 & 8.054 & 0.7869 \end{bmatrix}$$

$$B = \begin{bmatrix} 1.383 \times 10^{-6} & -9.384 \times 10^{-7} & -4.458 \times 10^{-7} \\ -69.59 & 47.64 & 22.43 \\ 18.64 & -11.71 & -6.657 \\ -36.13 & 22.83 & 13.06 \\ 68.76 & -46.78 & -22.12 \\ 3236 & 2437 & -1405 \end{bmatrix}$$

$$C = \begin{bmatrix} 0 & 0 & 0 & 0 & 0 & 1 \\ 0.4548 & 4.222 & 0 & 1.431 & 5.013 & 0.0007067 \end{bmatrix}$$

$$\mathrm{D} = 0$$

3. Experiment Apparatus

3.1. Catalyst Preparation

For the autothermal reforming, several institutions are dedicated to the development of catalysts. The $Pd/Zn/Al_2O_3$ catalyst exhibited a high activity and generated syngas with a CO concentration below 5 vol.% when the catalyst was heated from 350 to 450 °C, where the hydrogen concentration was close to 50 vol.% [47–49]. Takeishi et al. [50] proposed a sol-gel method to prepare the superior catalyst for the hydrocarbon reforming. Due to the close existence of the active sites for each reaction of the catalyst, its catalytic performance was better than that of the physically mixed dimethyl ether hydrolysis catalyst and methanol SR catalyst. In our experiments, 3.5 g of the $Pd/Zn/Al_2O_3$ catalyst prepared by the sol-gel method is coated on the surface of honeycomb cordierite ceramics with specific loadings of Pd, Zn and γ-Al_2O_3 of 5, 20 and 75 wt.%, respectively. Entire catalysts are made into a porous cylinder with a diameter of 36 mm and a length of 160 mm.

3.2. MPC Controller Design

Considering the diversity of the hydrogen generation systems, the main subject of this paper is the use of an MPC control scheme for the MIMO ATR reactors. Control of the hydrogen production rate and reactor temperature of the ATR reactor is achieved by specifically feeding air, dimethyl ether, and steam.

As shown in Figure 3, the implementation of the hydrogen production control system consists of three sections: feedstock supply module, autothermal reaction module, and signal acquisition and control module. Dimethyl ether and high-purity air are stored in two cylinders, and when the autothermal reaction proceeds, they are precisely fed to the reactor through two mass flow controllers (Ethernet, MKS Instruments, Andover, MA, USA) attached to the cylinders. At the same time, under the action of the syringe pump (Chemyx.Inc, Fusion100, Stafford, UK), the deionized water stored in the syringe is converted into steam and fed to the reformer through a steel pipe wrapped with an electric heating belt at 150°C to participate in the autothermal reaction. The hydrogen generated system prototype is shown in Figure 4.

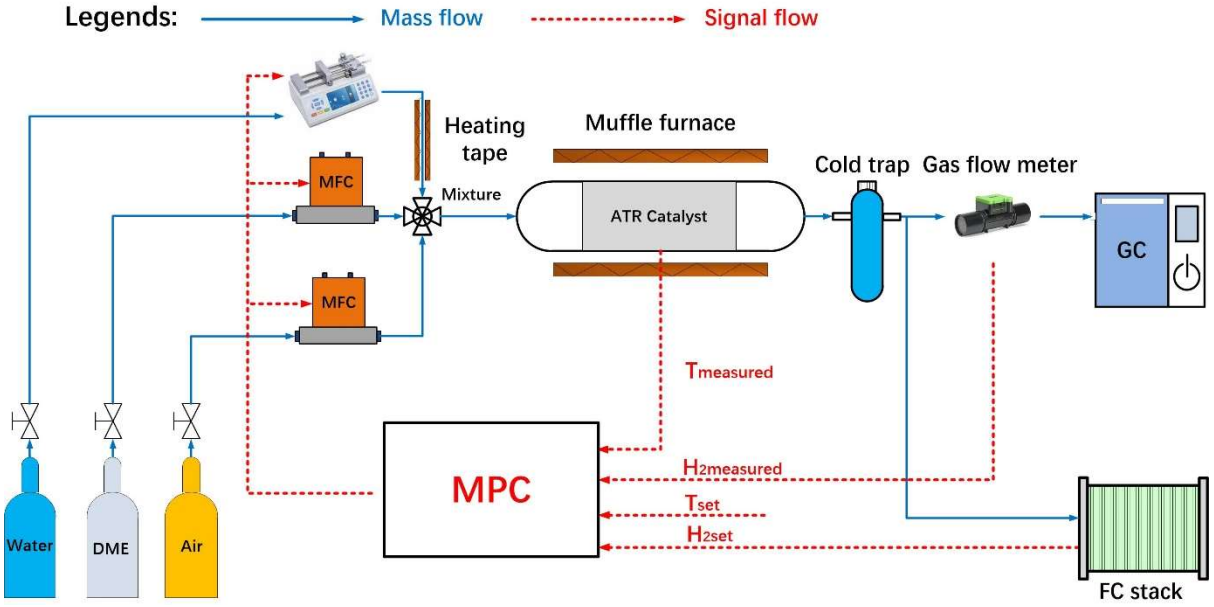

Figure 3. Schematic diagram of the controlled pilot plant unit for the hydrogen production system.

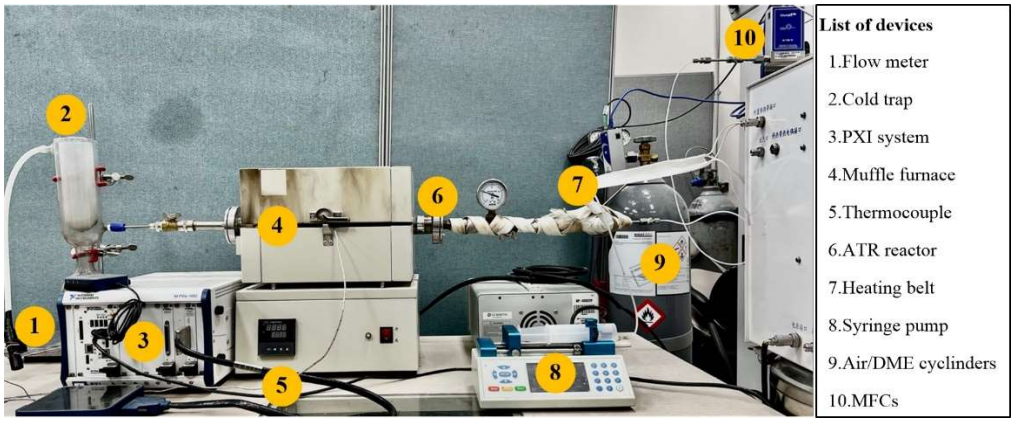

Figure 4. Hydrogen generation system prototype.

The autothermal reaction module is a fixed catalyst bed reactor formed by packing the catalyst mentioned in Section 3.1 in a reactor, which is made of a steel tube with an outer diameter of 40 mm and thickness of 2 mm. The reactor is enclosed in a tubular muffle furnace that provides heat to raise the catalyst temperature for the optimal catalytic activity and isolates the heat losses during the reaction. These measures can efficiently initialize the hydrogen production system and are beneficial to maintain the optimal temperature of the catalyst. A cold trap is attached to the reactor outlet to lower the temperature of the hydrogen-rich gas and condense the excess vapor in it because the subsequent gas flow meter and gas chromatograph (GC) measurements need to be performed in a normal temperature and dehydrated measurement environment. The GC can test the purity of a particular compound, separate the components in a mixture, and detect the relative amounts of each component. In this study, GC and a gas flow meter are used to test the molarity of hydrogen in the syngas and detect the hydrogen yield.

The signal acquisition and control module are developed, based on the model predictive control, where two mass flow controllers (MFCs) and one syringe pump are used to control the feed rates of the feedstocks. The NI device and LabVIEW 2019 are used to collect and process the temperature of the catalyst bed and the hydrogen yield. This type of interaction has a wide range of applications for its efficient and accurate properties. In the closed-loop control system, based on MPC, the reactor temperature T_{set} and hydrogen demand H_{2set} are two control objectives that need to be detected as real-time outputs of the system. Therefore, a K-type thermocouple (0–1300 °C) is attached to the reactor surface to detect the reaction temperature $T_{measured}$, and a flow meter (Sensirion AG Inc., SFM3020, Stäfa, Swizerland) is installed at the reactor outlet to detect the flow rate of the syngas F_P.

Due to the lack of a mechanism to detect the hydrogen flow rate online, this study obtained the general volume fraction φ_{H_2} of hydrogen through GC measurements in multiple experiments. Then, the hydrogen production rate can be calculated with Equations (14) and (15):

$$F_{H_2} = \left(F_P - F_{N_2}\right) \times \varphi_{H_2} \tag{14}$$

$$F_{N_2} = F_{Air} \times \varphi_{N_2} \tag{15}$$

where F_{H_2} denotes the hydrogen production rate; F_P is the flow rate of the syngas, which is detected by the gas flow meter; and F_{Air} is the flow rate of the high-purity air, which can be measured by the MFC. φ_{N_2} denotes the nitrogen volume fraction in the high-purity air, which is 79%.

φ_{H_2} is the hydrogen volume fraction in the syngas. According to previous research results [34], the volume fraction of hydrogen is mainly affected by the reaction temperature and the concentration of each component, which does not change drastically in the operation. The effect of the reaction temperature on the hydrogen production is also fully explored through the experiment and simulation. As shown in Figure 5, the hydrogen content reaches the maximum value of 43% while the reactor temperature is approximately

400 °C. Therefore, according to the measurements of the GC, and considering the necessary hydrogen redundancy, the general hydrogen volume fraction φ_{H_2} in the syngas is determined as 40%, while the optimal temperature of the autothermal reforming is 400 °C.

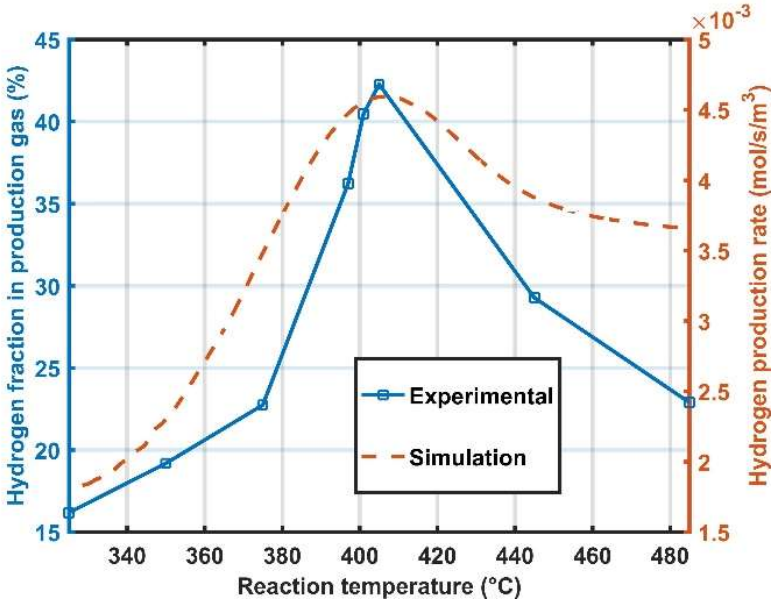

Figure 5. Schematic diagram of the hydrogen volume fraction under temperature variation.

4. Result Discussion

The developed MPC was tested to verify the tracking performance of the desired hydrogen yield and the anti-disturbance of the catalyst temperature in the reactor-specific hydrogen demand profile. The dynamic behavior of the hydrogen yield and catalyst temperature with a step change in the set signal was also investigated.

Figure 6 shows the hydrogen demand profile in a control system with two MFCs and a syringe pump as actuators. The set hydrogen demand flow rate presents a step change from 0.09 mol/min to 0.23 mol/min. The corresponding flow rates of DME, high-purity air, and liquid water in both the simulation and experiment are shown in Figure 7. To achieve the control objectives, the MPC control strategy implemented in LabVIEW and the results obtained in the simulation show similar corresponding control actions, according to the changes in the hydrogen demand curve.

Based on the control actions of the MPC and the working characteristics of the actuators, the dynamic response of DME and a high-purity air show certain overshoot fluctuations when the set signal changes, but after approximately 20 s of the MPC modulation, the system reaches a stable state, while the liquid water flow provided by the syringe pump rises more smoothly. The experimental results show a slightly larger overshoot and slightly longer steady-state arrival time during the dynamic changes, compared to the simulation results, but within an acceptable range. The steam-to-carbon ratio (SCR) and oxygen-to-carbon ratio (OCR) in the reaction changed due to the different fluctuations among the components. Thus, the thermal neutrality of the entire autothermal reforming reaction is guaranteed in the dynamic operation and is beneficial for maintaining a stable reactor temperature.

The dashed line in Figure 8 shows the hydrogen flow rate obtained from the simulation, and the solid line represents the hydrogen generation curve in the experiment. This curve is calculated, based on the detection of the mass flow meter and Equations (13) and (14). The simulation result shows that the overshoot of the hydrogen flow rate during the dynamic response process does not exceed 0.004 mol/min. Furthermore, the measured hydrogen generation rate fluctuates, due to the operating error of the flowmeter and the influence of the turbulent flow in the pipeline. However, these factors are not significant with respect to

the overall change of hydrogen flow. Based on these results, the traceability of the hydrogen yield is validated, and the dynamic behavior of the controller indicates that the setpoint tracking is satisfactory.

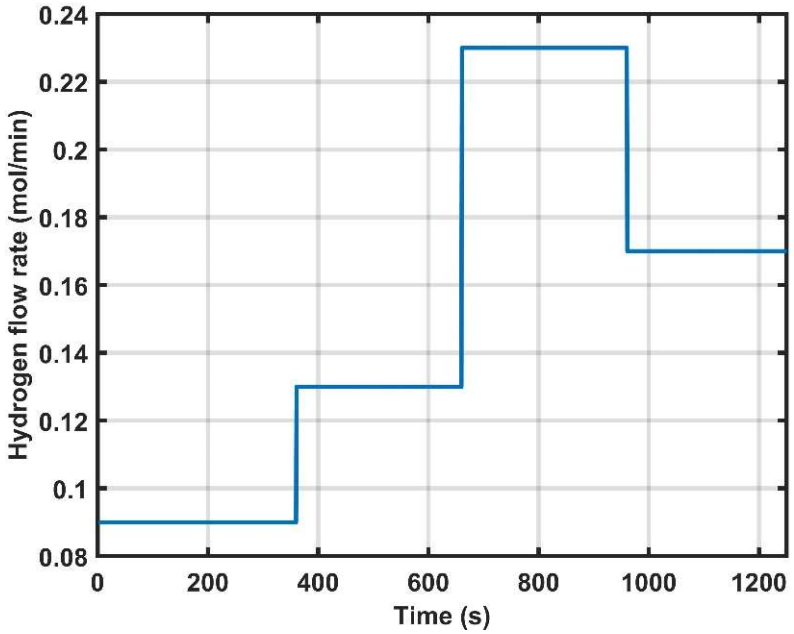

Figure 6. Schematic diagram of the hydrogen demand profile.

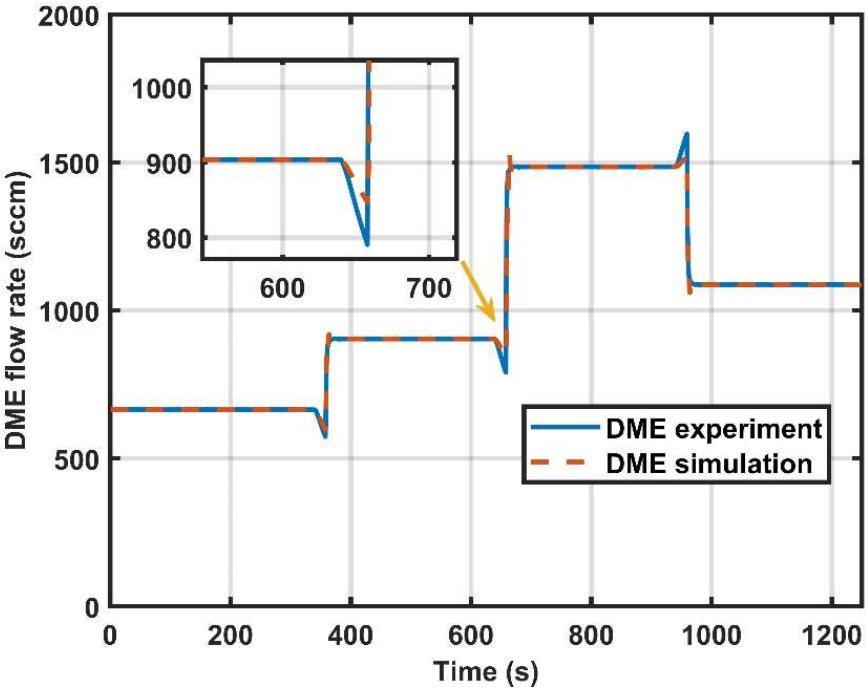

(**a**)

Figure 7. *Cont.*

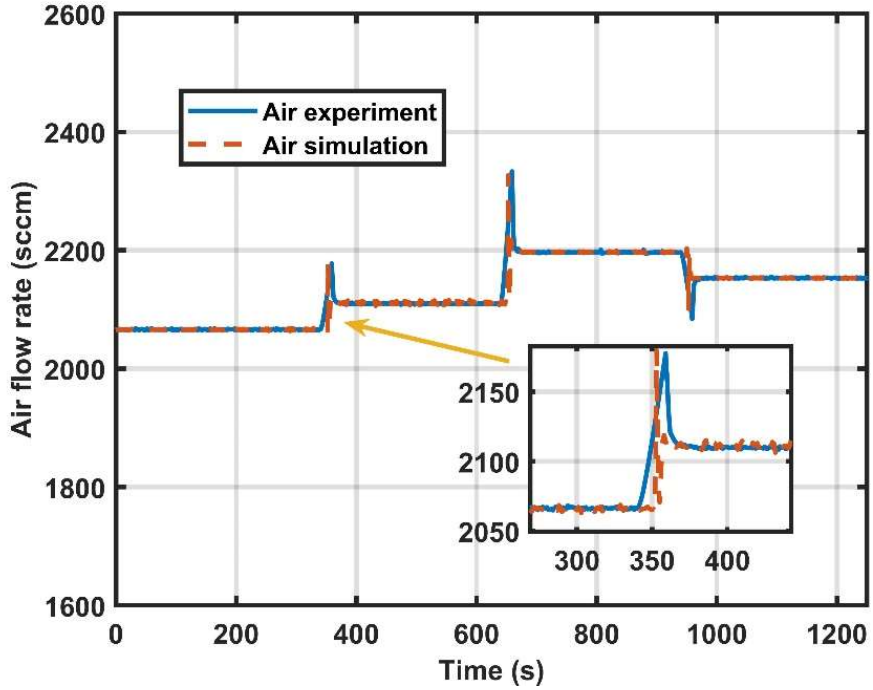

(**b**)

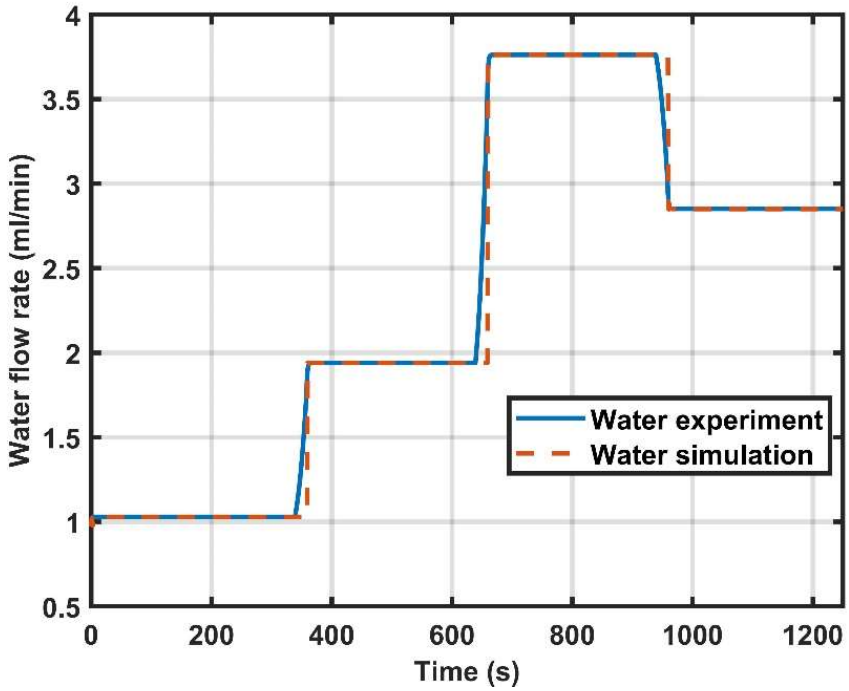

(**c**)

Figure 7. Schematic diagram of the feedstocks supply rate profile ((**a**) DME; (**b**) High-purity air; (**c**) Water).

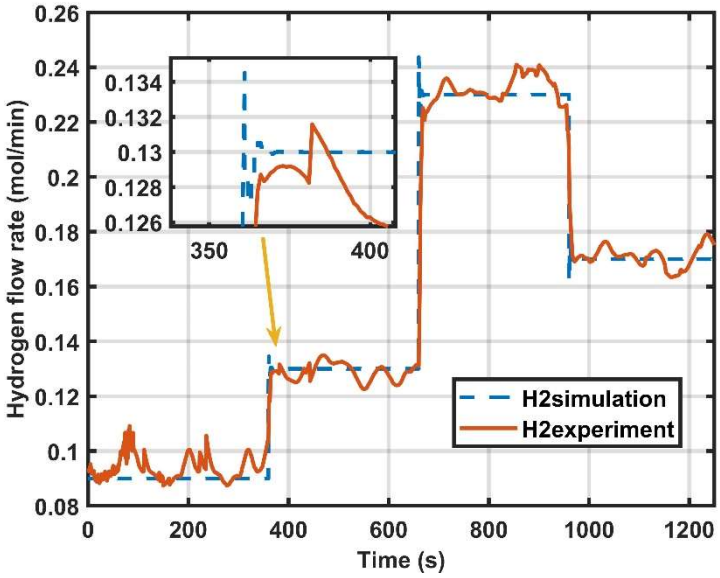

Figure 8. Schematic diagram of the simulation and experiment hydrogen flow rate.

The reactor temperature has a considerable effect on the catalyst activity. In the dynamic control, it should exhibit an excellent anti-disturbance with the continuous change of the hydrogen production rate to ensure that the autothermal reforming reaction is conducted at an optimal temperature. Figure 9a shows the variation profile of the catalyst temperature obtained from the simulation and experimental measurements in the MPC control. Figure 9b presents the experimental temperature result obtained in the PID control, as reported in previous research [41]. Based on the similar changes in the hydrogen demand curve, both control mechanisms can keep the catalyst temperature at the optimum value of 400 °C, but the temperature curve is smoother in the MPC control strategy. Only a slight perturbation occurs when the set hydrogen demand curve changes in steps. This dynamic performance shows that the anti-disturbance of the catalyst temperature is satisfactory.

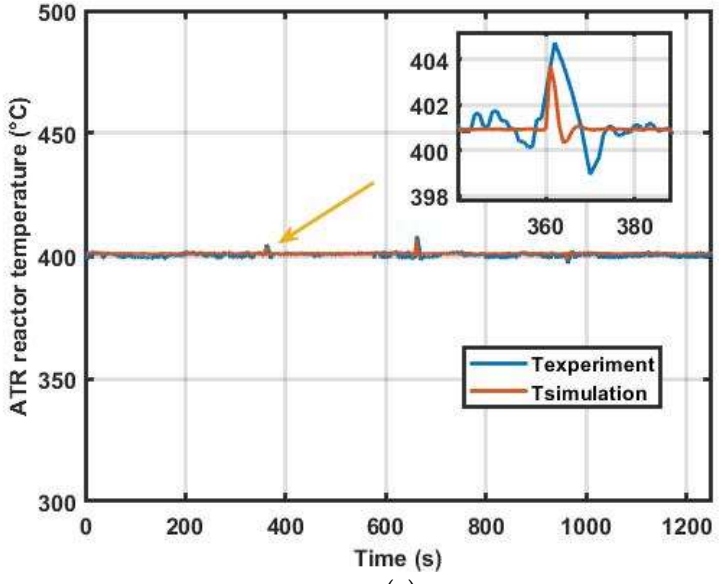

(**a**)

Figure 9. *Cont.*

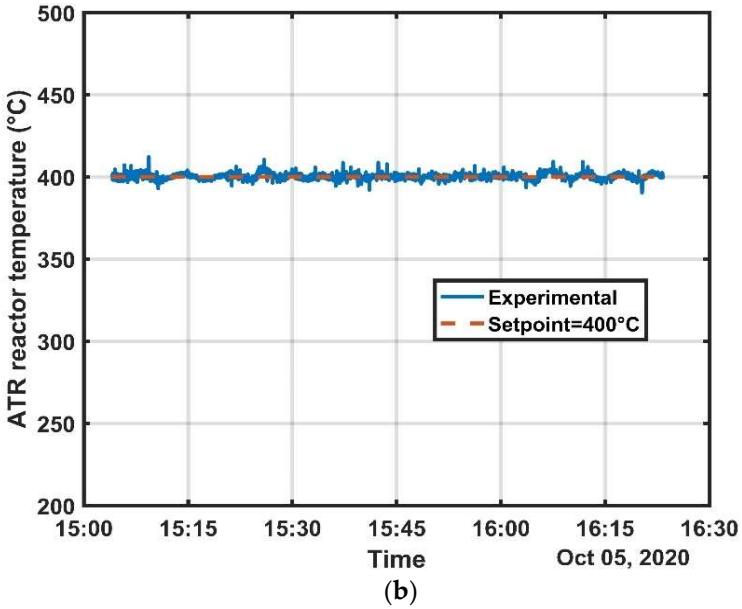

Figure 9. Schematic diagram of the reactor temperature profile ((**a**) MPC control; (**b**) PID control).

5. Conclusions

In this study, a rigorous mathematical model was proposed to the simulate and control the DME autothermal reformer. An advanced MPC scheme was implemented, which calculated the optimal sequence of the controlled variables within a specified prediction horizon. The experiment and simulation results indicated that:

1. The expected dynamic response of the hydrogen production rate was achieved by controlling the feed rate of dimethyl ether in the range of 0.09–0.23 mol/min, and a high purity air and steam as feedstocks. The traceability of the hydrogen production rate was satisfactory.

2. The disturbance compensation was obtained for maintaining the catalyst temperature stability. The catalyst temperature shows a good immunity to the feedstock flow rate variations. Although a deviation of the catalyst temperature of about 4 °C occurred during the step change of the feedstock flow rate, it recovered to the control target value within a short time domain (20 s).

Based on these results, the next step of the study is to further improve the purity and production efficiency of hydrogen and to integrate this hydrogen generation system with the PEMFCs to develop a complete energy management system.

Author Contributions: Formal analysis, T.-Q.Z.; Investigation, S.J.; Project administration, Y.-B.K. All authors have read and agreed to the published version of the manuscript.

Funding: This work was supported by the National Research Foundation of Republic of Korea (22R1I1A3063283).

Conflicts of Interest: The authors declare no conflict of interest.

References

1. Liu, J.; Tan, J.; Yang, W.; Li, Y.; Wang, C. Better electrochemical performance of PEMFC under a novel pneumatic clamping mechanism. *Energy* **2021**, *229*, 120796. [CrossRef]
2. Chiu, W.C.; Hou, S.S.; Chen, C.Y.; Lai, W.H.; Horng, R.F. Hydrogen-rich gas with low-level CO produced with autothermal methanol reforming providing a real-time supply used to drive a kW-scale PEMFC system. *Energy* **2022**, *239*, 122267. [CrossRef]
3. Yang, B.; Li, D.; Zeng, C.; Chen, Y.; Guo, Z.; Wang, J.; Shu, H.; Yu, T.; Zhu, J. Parameter extraction of PEMFC via Bayesian regularization neural network based meta-heuristic algorithms. *Energy* **2021**, *228*, 120592. [CrossRef]
4. Karayel, G.K.; Javani, N.; Dincer, I. Effective use of geothermal energy for hydrogen production, A comprehensive application. *Energy* **2022**, *249*, 123597. [CrossRef]

5. Kafetzis, A.; Ziogou, C.; Papadopoulou, S.; Voutetakis, S.; Seferlis, P. Nonlinear Model Predictive Control of an Autonomous Power System Based on Hydrocarbon Reforming and High Temperature Fuel Cell. *Energies* **2021**, *14*, 1371. [CrossRef]
6. Liu, J.; Yang, Q.; Ou, S.; Liu, J. Factor decomposition and the decoupling effect of carbon emissions in China's manufacturing high-emission subsectors. *Energy* **2022**, *248*, 123568. [CrossRef]
7. Takach, M.; Sarajlić, M.; Peters, D.; Kroener, M.; Schuldt, F.; Maydell, K. Review of Hydrogen Production Techniques from Water Using Renewable Energy Sources and Its Storage in Salt Caverns. *Energies* **2022**, *15*, 1415. [CrossRef]
8. Sharma, P.; Sahoo, B.B. Precise prediction of performance and emission of a waste derived Biogas–Biodiesel powered Dual–Fuel engine using modern ensemble Boosted regression Tree: A critique to Artificial neural network. *Fuel* **2022**, *321*, 124131. [CrossRef]
9. Shafiei, E.; Davidsdottir, B.; Leaver, J.; Stefansson, H.; Asgeirsson, E.I. Energy, economic, and mitigation cost implications of transition toward a carbon-neutral transport sector, A simulation-based comparison between hydrogen and electricity. *J. Clean. Prod.* **2017**, *141*, 237–247. [CrossRef]
10. Dawood, F.; Anda, M.; Shafiullah, G.M. Hydrogen production for energy, An overview. *Energy* **2020**, *45*, 3847–3869. [CrossRef]
11. Kalinci, Y.; Hepbasli, A.; Dincer, I. Techno-economic analysis of a stand-alone hybrid renewable energy system with hydrogen production and storage options. *Int. J. Hydrog. Energy* **2015**, *40*, 7652–7664. [CrossRef]
12. Acar, C.; Dincer, I. Review and evaluation of hydrogen production options for better environment. *J. Clean. Prod.* **2019**, *218*, 835–849. [CrossRef]
13. Ahmed, A.; Al-Amin, A.Q.; Ambrose, A.F.; Saidur, R. Hydrogen fuel and transport system, A sustainable and environmental future. *Int. J. Hydrog. Energy* **2016**, *41*, 1369–1380. [CrossRef]
14. Hou, T.F.; Shanmugasundaram, A.; Hassan, M.A.; Johar, M.A.; Ryu, S.W.; Lee, D.W. ZnO/Cu_2O-decorated rGO, heterojunction photoelectrode with improved solar water splitting performance. *Int. J. Hydrog. Energy* **2019**, *44*, 19177–19192. [CrossRef]
15. Bellotti, D.; Rivarolo, M.; Magistri, L.; Massardo, A.F. Feasibility study of methanol production plant from hydrogen and captured carbon dioxide. *J. CO2 Util.* **2017**, *21*, 132–138. [CrossRef]
16. Zou, W.J.; Shen, K.Y.; Jung, S.; Kim, Y.B. Application of thermoelectric devices in performance optimization of a domestic PEMFC-based CHP system. *Energy* **2021**, *229*, 120698. [CrossRef]
17. Ou, K.; Wang, Y.X.; Li, Z.Z.; Shen, Y.D.; Xuan, D.J. Feedforward fuzzy-PID control for air flow regulation of PEM fuel cell system. *Int. J. Hydrog. Energy* **2015**, *40*, 11686–11695. [CrossRef]
18. Bianchini, M.; Alayo, N.; Soler, L.; Salleras, M.; Fonseca, L.; Llorca, J.; Tarancón, A. Standalone micro-reformer for on-demand hydrogen production from dimethyl ether. *J. Power Sources* **2021**, *506*, 230241. [CrossRef]
19. Brown, L.F. A comparative study of fuels for on-board hydrogen production for fuel-cell-powered automobiles. *Int. J. Hydrog. Energy* **2001**, *26*, 381–397. [CrossRef]
20. Faungnawakij, K.; Tanaka, Y.; Shimoda, N.; Fukunaga, T.; Kikuchi, R.; Eguchi, K. Hydrogen production from dimethyl ether steam reforming over composite catalysts of copper ferrite spinel and alumina. *Appl. Catal. B-Environ.* **2007**, *74*, 144–151. [CrossRef]
21. Choi, S.; Bae, J. Autothermal reforming of dimethyl ether with CGO-based precious metal catalysts. *J. Power Sources* **2016**, *307*, 351–357. [CrossRef]
22. Tartakovsky, L.; Mosyak, A.; Zvirin, Y. Energy analysis of ethanol steam reforming for hybrid electric vehicle. *Int. J. Energy Res.* **2013**, *37*, 259–267. [CrossRef]
23. Malik, F.R.; Kim, Y.B. Autothermal reforming of n-hexadecane over Rh catalyst to produce syngas in microchannel reactor using finite element method. *Int. J. Energy Res.* **2019**, *43*, 779–790. [CrossRef]
24. Nwosu, C.; Ayodele, O.; Ibrahim, H. Optimization of hydrogen production via catalytic autothermal reforming of crude glycerol using response surface methodology and artificial neural network. *Int. J. Energy Res.* **2021**, *45*, 18999–19013. [CrossRef]
25. Teng, C.Y.; Chiu, S.J. Hydrogen production by partial oxidation of ethanol over Pt/CNT catalysts. *Int. J. Energy Res.* **2013**, *37*, 1689–1698. [CrossRef]
26. Wu, Z.; Guo, Z.; Yang, J.; Wang, Q. Effect of diameter distribution of particles on methane steam reforming in multi-channel grille-sphere composite packed bed. *Energy Conv. Manag.* **2022**, *265*, 115764. [CrossRef]
27. Cherif, A.; Nebbali, R.; Sen, F.; Sheffield, J.W.; Doner, N.; Nasseri, L. Modeling and simulation of steam methane reforming and methane combustion over continuous and segmented catalyst beds in autothermal reactor. *Int. J. Hydrog. Energy* **2022**, *47*, 9127–9138. [CrossRef]
28. Faungnawakij, K.; Viriya-Empikul, N.; Tanthapanichakoon, W. Evaluation of the thermodynamic equilibrium of the autothermal reforming of dimethyl ether. *Int. J. Hydrog. Energy* **2011**, *36*, 5865–5874. [CrossRef]
29. Wu, Z.; Aguirre, A.; Tran, A.; Durand, H.; Ni, D.; Christofides, P.D. Model predictive control of a steam methane reforming reactor described by a computational fluid dynamics model. *Ind. Eng. Chem. Res.* **2017**, *56*, 6002–6011. [CrossRef]
30. Wang, H.S.; Chang, C.P.; Huang, Y.J.; Su, Y.C.; Tseng, F.G. A high-yield and ultra-low-temperature methanol reformer integratable with phosphoric acid fuel cell (PAFC). *Energy* **2017**, *133*, 1142–1152. [CrossRef]
31. Pantoleontos, G.; Kikkinides, E.S.; Georgiadis, M.C. A heterogeneous dynamic model for the simulation and optimisation of the steam methane reforming reactor. *Int. J. Hydrog. Energy* **2012**, *37*, 16346–16358. [CrossRef]
32. Ubago-Pérez, R.; Carrasco-Marín, F.; Moreno-Castilla, C. Methanol partial oxidation on carbon-supported Pt and Pd catalysts. *Catal. Today* **2007**, *123*, 158–163. [CrossRef]
33. Dolanc, G.; Pregelj, B.; Petrovčič, J.; Pasel, J.; Kolb, G. Control of autothermal reforming reactor of diesel fuel. *J. Power Sources* **2016**, *313*, 223–232. [CrossRef]

34. Khalid, M.; Savkin, A.V. A model predictive control approach to the problem of wind power smoothing with controlled battery storage. *Renew. Energy* **2010**, *35*, 1520–1526. [CrossRef]
35. Kyriakides, S.; Seferlis, P.; Voutetakis, S.; Papadopoulou, S. Model predictive control for hydrogen production in a membrane methane steam reforming reactor. *Chem. Eng. Trans.* **2016**, *52*, 991–996.
36. Paliwal, N.K.; Singh, A.K.; Singh, N.K. Short-term optimal energy management in stand-alone microgrid with battery energy storage. *Arch. Electr. Eng.* **2018**, *67*, 499–513.
37. Hu, Y.; Chmielewski, D.J. Nonlinear multivariable predictive control of an autothermal reforming reactor for fuel cell applications. In Proceedings of the 2009 American Control Conference, St. Louis, MO, USA, 10–12 June 2009; pp. 659–664.
38. Wang, J.; Chen, H.; Tian, Y.; Yao, M.; Li, Y. Thermodynamic analysis of hydrogen production for fuel cells from oxidative steam reforming of methanol. *Fuel* **2012**, *97*, 805–811. [CrossRef]
39. Li, Y.; Fu, Q.; Flytzani-Stephanopoulos, M. Low-temperature water-gas shift reaction over Cu-and Ni-loaded cerium oxide catalysts. *Appl. Catal. B-Environ.* **2000**, *27*, 179–191. [CrossRef]
40. LeValley, T.L.; Richard, A.R.; Fan, M. The progress in water gas shift and steam reforming hydrogen production technologies–A review. *Int. J. Hydrog. Energy* **2014**, *39*, 16983–17000. [CrossRef]
41. Zhang, T.Q.; Malik, F.R.; Jung, S.; Kim, Y.B. Hydrogen production and temperature control for DME autothermal reforming process. *Energy* **2022**, *239*, 121980. [CrossRef]
42. Ouzounidou, M.; Ipsakis, D.; Voutetakis, S.; Papadopoulou, S.; Seferlis, P. A combined methanol autothermal steam reforming and PEM fuel cell pilot plant unit: Experimental and simulation studies. *Energy* **2009**, *34*, 1733–1743. [CrossRef]
43. Ipsakis, D.; Voutetakis, S.; Papadopoulou, S.; Seferlis, P. Optimal operability by design in a methanol reforming-PEM fuel cell autonomous power system. *Int. J. Hydrog. Energy* **2012**, *37*, 16697–16710. [CrossRef]
44. Nilsson, M.; Jozsa, P.; Pettersson, L.J. Evaluation of Pd-based catalysts and the influence of operating conditions for autothermal reforming of dimethyl ether. *Appl. Catal. B-Environ.* **2007**, *76*, 42–50. [CrossRef]
45. Wang, J.; Wei, S.; Wang, Q.; Sundén, B. Transient numerical modeling and model predictive control of an industrial-scale steam methane reforming reactor. *Int. J. Hydrog. Energy* **2021**, *46*, 15241–15256. [CrossRef]
46. Zecevic, N.; Bolf, N. Advanced operation of the steam methane reformer by using gain-scheduled model predictive control. *Ind. Eng. Chem. Res.* **2020**, *59*, 3458–3474. [CrossRef]
47. Ismagilov, I.Z.; Matus, E.V.; Kuznetsov, V.V.; Mota, N.; Navarro, R.M.; Kerzhentsev, M.A.; Ismagilov, Z.R.; Fierro, J.L.G. Nanoscale control during synthesis of Me/La_2O_3, $Me/Ce_xGd_{1-x}O_y$ and $Me/Ce_xZr_{1-x}O_y$ (Me = Ni, Pt, Pd, Rh) catalysts for autothermal reforming of methane. *Catal. Today* **2013**, *210*, 10–18. [CrossRef]
48. Ledesma, C.; Llorca, J. $CuZn/ZrO_2$ catalytic honeycombs for dimethyl ether steam reforming and autothermal reforming. *Fuel* **2013**, *104*, 711–716. [CrossRef]
49. Nilsson, M.; Jansson, K.; Jozsa, P.; Pettersson, L.J. Catalytic properties of Pd supported on $ZnO/ZnAl_2O_4/Al_2O_3$ mixtures in dimethyl ether autothermal reforming. *Appl. Catal. B-Environ.* **2009**, *86*, 18–26. [CrossRef]
50. Takeishi, K.; Akaike, Y. Hydrogen production by dimethyl ether steam reforming over copper alumina catalysts prepared using the sol–gel method. *Appl. Catal. A-Gen.* **2016**, *510*, 20–26. [CrossRef]